

A yeast-based screen reveals that sulfasalazine inhibits tetrahydrobiopterin biosynthesis

Christopher Chidley, Hirohito Haruki, Miriam Grønlund Pedersen, Evelyne Muller & Kai Johnsson*

We introduce an approach for detection of drug-protein interactions that combines a new yeast three-hybrid screening for identification of interactions with affinity chromatography for their unambiguous validation. We applied the methodology to the profiling of clinically approved drugs, resulting in the identification of previously known and unknown drug-protein interactions. In particular, we were able to identify off-targets for erlotinib and atorvastatin, as well as an enzyme target for the anti-inflammatory drug sulfasalazine. We demonstrate that sulfasalazine and its metabolites, sulfapyridine and mesalamine, are inhibitors of the enzyme catalyzing the final step in the biosynthesis of the cofactor tetrahydrobiopterin. The interference with tetrahydrobiopterin metabolism provides an explanation for some of the beneficial and deleterious properties of sulfasalazine and furthermore suggests new and improved therapies for the drug. This work thus establishes a powerful approach for drug profiling and provides new insights in the mechanism of action of clinically approved drugs.

Most small-molecule drugs elicit their therapeutic activity by interfering with the function of one or more proteins by physically binding to them. The identification of all protein targets of a drug therefore provides the basis for the understanding of its beneficial or deleterious actions. However, the identification of drug-protein interactions remains a challenging task, as testified to by the fact that the primary targets of various clinically approved drugs remain unknown. Numerous strategies have been developed to directly or indirectly identify the targets of bioactive small molecules^{1,2}. The most popular approach to directly identify drug-protein interactions relies on affinity chromatography using an immobilized drug. Chemical proteomics, which associates affinity chromatography with mass spectrometry detection, is widely used for drug profiling³. Despite various technical advances³, the use of chemical proteomics nevertheless remains difficult for identification of low-abundance target proteins or proteins with low solubility or stability in cell extracts. There is therefore a generally acknowledged need for alternative approaches to identify drug-protein interactions.

Here we describe an approach for drug profiling combining an improved yeast three-hybrid (Y3H) system for identification of drug-protein interactions with affinity chromatography for unambiguous validation of binding. We applied the approach to the profiling of clinically approved drugs, resulting in identification of known and unknown drug-protein interactions.

RESULTS

A Y3H system based on SNAP-tag labeling

The Y3H system is a modified version of the yeast two-hybrid (Y2H) system adapted for detection of drug-protein interactions. It requires derivatization of the drug of interest with a ligand that can be anchored to a DNA-binding protein inside yeast cells; the interaction of the anchored drug with a target protein is then detected by linking their association to the transcriptional activation of a reporter gene⁴. Attractive features of this drug profiling approach include (i) the availability of diverse cDNA libraries from different tissues and organisms, (ii) the possibility of directly identifying the drug-binding domains of proteins, (iii) the possibility of detecting

low-abundance proteins and (iv) its experimental simplicity. However, although promising initial results have been obtained^{4,5}, the Y3H system has scarcely been used for drug profiling. Possible reasons for this scarce use include (i) the need to couple the drug of interest to a specific ligand, (ii) the low uptake of synthetic molecules into yeast and the associated low sensitivity of the Y3H system, as well as (iii) the large number of false positives coming out of screenings and the ensuing difficulty in identifying true interactions amongst false positives.

We based our Y3H system on the covalent labeling of SNAP-tag fusion proteins inside yeast cells by *O*⁶-benzylguanine (BG) derivatives⁶ (Fig. 1a). BG derivatives can be directly coupled to a variety of functional groups, facilitating the required derivatization of the drug (Supplementary Methods). To establish SNAP-tag-based Y3H screening as a robust and easy-to-use tool for drug profiling, we first developed and characterized a system that addresses the shortcomings of previous strategies.

Development of a sensitive SNAP-tag-based Y3H system

The extent of SNAP-tag labeling with the drug of interest depends on the intracellular concentration of the drug derivative. We hypothesized that an increase in such intracellular concentration would yield a corresponding increase in sensitivity of the SNAP-tag-based Y3H system. The intracellular accumulation of drugs in *Saccharomyces cerevisiae* is frequently hindered by an efficient multidrug-resistance mechanism. Yeast cells express a variety of ATP-binding cassette transporters that confer drug resistance when overexpressed or hypersensitivity when deleted. We therefore deleted three genes (PDR5, SNQ2 and YOR1) encoding broad-spectrum drug transporters from the genome of a commercially available Y3H reporter yeast strain (Supplementary Results and Supplementary Methods). Indeed, it has been shown that triple deletion of PDR5, SNQ2 and YOR1 increases the sensitivity of yeast to an extremely broad range of compounds⁷; furthermore, the labeling of SNAP-tag fusion proteins in yeast cells with fluorescent BG derivatives is efficient in a yeast strain with the same three deletions⁸. We quantified SNAP-tag labeling in the triple deletion reporter strain (1A2) and compared it to that of the unmodified reporter strain (NMY51).

*Institute of Chemical Sciences and Engineering, Institute of Bioengineering, National Centre of Competence in Research Chemical Biology, École Polytechnique Fédérale de Lausanne, Lausanne, Switzerland. *e-mail: kai.johnsson@epfl.ch

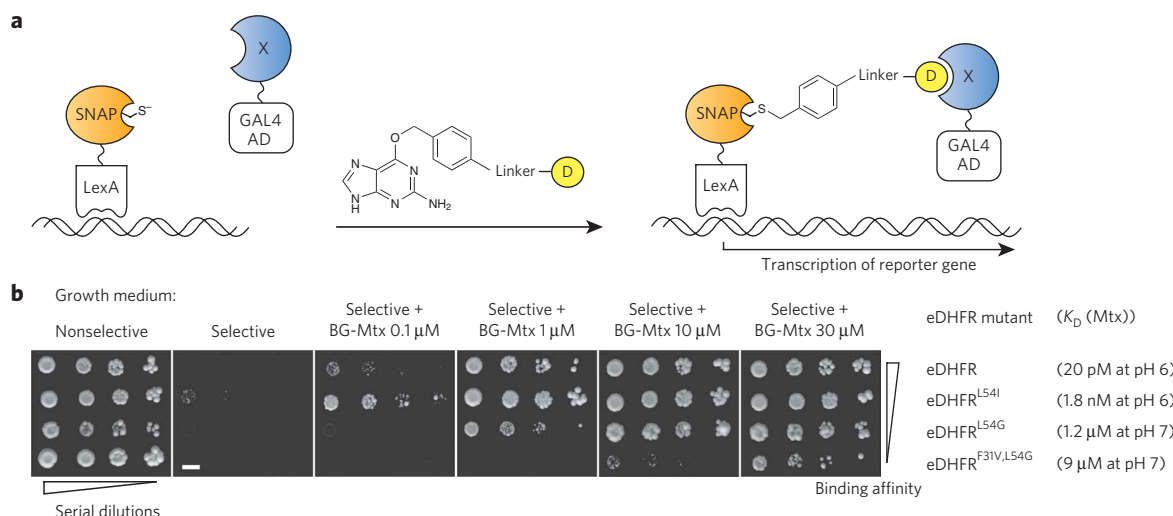


Figure 1 | A Y3H system based on SNAP-tag labeling. (a) Illustration of the SNAP-tag-based Y3H system developed for identification of drug-protein interactions. A BG derivative of the drug of interest (D) covalently labels SNAP-tag in living yeast cells. The interaction of the covalently anchored drug with a target protein (X) is detected by linking their association to the transcriptional activation of a reporter gene. (b) Characterization of the sensitivity of the system by analysis of the Y3H growth induced by drug-protein interactions of defined affinity. The binding of methotrexate (Mtx) to *E. coli* DHFR (eDHFR) can be modified by the introduction of point mutations to cover a wide range of binding affinities. The mentioned binding affinities are published values for the binding of underivatized methotrexate to eDHFR or to an eDHFR mutant^{11,12}. Yeast cells coexpressing LexA-SNAP and GAL4AD-eDHFR (or GAL4AD-eDHFR mutant) were spotted on growth medium selective for reporter gene activation at different concentrations of a BG-methotrexate derivative (BG-Mtx). Scale bar, 5 mm.

We observed that triple deletion of PDR5, SNQ2 and YOR1 increases the labeling efficiency of different BG drug derivatives up to four-fold (Supplementary Fig. 2a–d).

In order to characterize the sensitivity of our Y3H system in the 1A2 strain, we performed model studies based on the binding of methotrexate to *E. coli* dihydrofolate reductase (eDHFR). We chose this interaction because it has been shown that derivatization of methotrexate at its glutamyl γ -carboxyl group does not affect binding to eDHFR⁹ and that a BG derivative of methotrexate (BG-Mtx) dimerizes SNAP-tag and eDHFR in yeast¹⁰. Furthermore, the binding strength of methotrexate to eDHFR can be modulated by single point mutations. In addition to wild-type eDHFR, we prepared three mutants that cover a wide range of binding affinities (K_D from 20 pM to 9 μ M)^{11,12}. We then tested the Y3H growth induced by coexpression of SNAP-tag and eDHFR fusion proteins at different concentrations of BG-Mtx (Fig. 1b). We were able to detect the interaction of methotrexate with eDHFR^{F31V,L54G} ($K_D = 9 \mu$ M), indicating that the sensitivity of the SNAP-tag-based Y3H system presented here is in the low micromolar range. We next compared the performance of 1A2 to that of NMY51 and observed that the deletion of PDR5, SNQ2 and YOR1 increases significantly the sensitivity of the SNAP-tag-based Y3H system (Supplementary Fig. 3).

Elimination of false positives

The use of cDNA libraries in Y2H and Y3H screenings often results in the isolation of false positives, mainly due to the presence of hybrid proteins expressed in the wrong reading frame or from untranslated regions of mRNA¹³. Methods have been developed that minimize the occurrence of false positives either by increasing the stringency of the system or by providing efficient ways of combing out non-specific interactions¹⁴; however, such increase in stringency is often at the expense of sensitivity. In the SNAP-tag-based Y3H system, we use two successive strategies for false positive elimination.

In a first step, the number of false positive colonies inherent to cDNA library screenings can be reduced by negative selection against unspecific interactions in the absence of drug derivative. Specifically, the anti-metabolite 5-fluoroorotic acid (5-FOA) can be

used to select against unspecific interactions that activate the URA3 reporter gene in the 1A2 strain in the absence of drug derivative, as the product of the URA3 gene transforms 5-FOA into a toxic compound (Supplementary Fig. 4a–c). We tested the efficacy of such a negative selection round in model screenings and observed a reduction in the number of unspecific interactions by a factor of 30 to 70, suggesting that a negative selection step should effectively lower the number of false positive colonies in cDNA library screenings (Supplementary Fig. 5a–c).

In a second step, false positives arising after positive selection can be eliminated in a simple respotting assay in which yeast growth is measured both in the presence and absence of the drug derivative, as only the growth of yeast cells containing true interactions is dependent on the presence of the drug derivative (Fig. 2a).

Verification of interactions

The verification of interactions is a difficult task in Y2H and Y3H screenings. To address this bottleneck, we established a strategy for an effective pulldown assay that utilizes the same BG drug derivative as used in the Y3H screenings (Fig. 2b). Specifically, the BG drug derivative is coupled to a glutathione S-transferase (GST)-SNAP fusion protein and the target protein transiently expressed with an epitope tag in mammalian cells. Pulldowns using glutathione beads in the presence and absence of underivatized drug and subsequent detection of the epitope-tagged protein through western blotting permit a rapid validation of the binding of the underivatized drug to the target protein. Furthermore, the same BG drug derivatives can be used to validate interactions by affinity chromatography of endogenous proteins.

Profiling of clinically approved drugs

Clinically approved drugs covering different therapeutic areas were subjected to our Y3H screening system after being derivatized with BG (Table 1 and Supplementary Fig. 6a). These approved drugs include extensively profiled drugs, such as the kinase inhibitors dasatinib and erlotinib, and drugs with obscure mechanisms of action, such as the anti-inflammatory agent sulfasalazine. Although

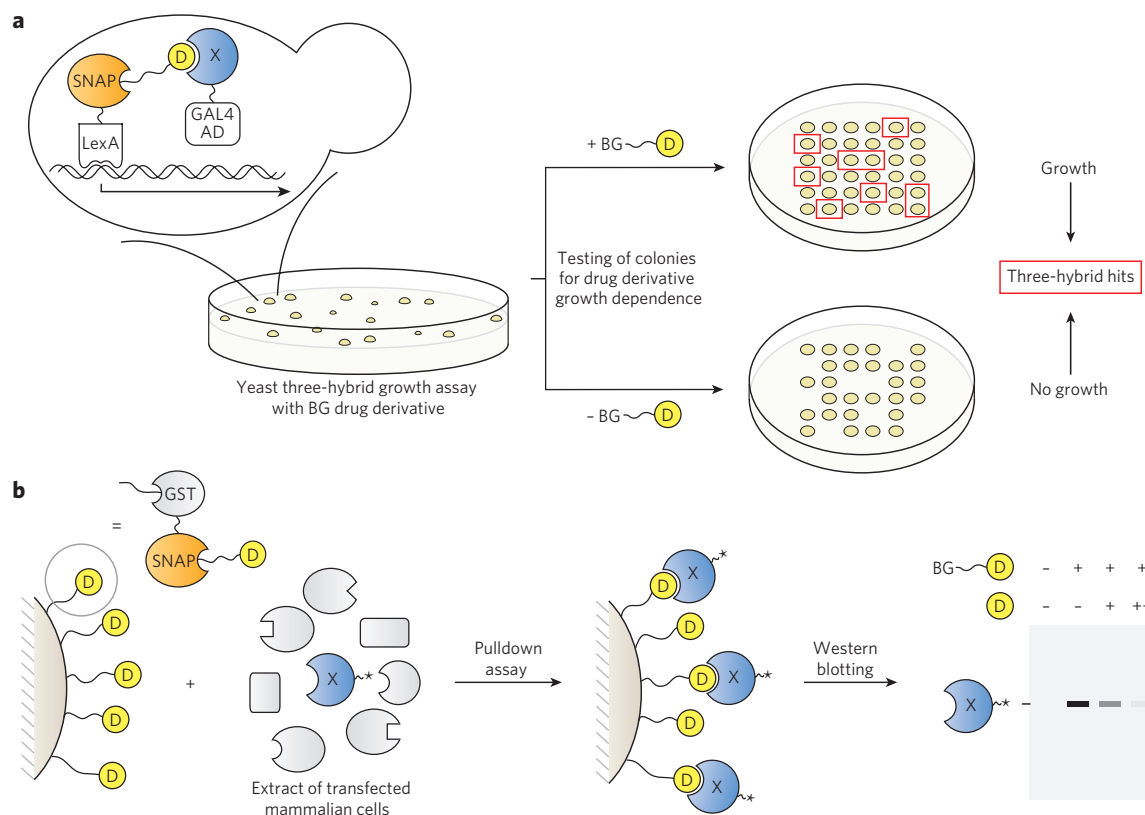


Figure 2 | Illustration of the yeast-based platform for drug profiling. (a) The SNAP-tag-based Y3H system allows the screening of human cDNA libraries for identification of the target(s) of small-molecule drugs (D). Yeast cells coexpressing LexA-SNAP and GAL4AD-X (X: cDNA library clone) are spread on growth medium selective for reporter gene activation and in the presence of a BG derivative of the drug of interest (BG-D). Specific Y3H hits are identified by testing all colonies growing on the selection plates for dependence on the presence of BG-D for growth on selective medium. The identities of the Y3H hits are determined by sequencing of the cDNA inserts and subsequent BLAST analysis. (b) Independent validation of the binding of the drug of interest to a target protein by affinity chromatography using the same drug derivative. A drug affinity matrix is prepared by immobilization of a GST-SNAP fusion protein on glutathione beads and subsequent reaction of SNAP-tag with BG-D. An epitope-tagged (*) target protein is overexpressed in mammalian cells. The specific binding of the target protein from a cell extract to the immobilized drug can be detected by western blotting. The binding of the underivatized drug to the target protein can be identified through competition experiments as shown in the schematic.

in some cases (atorvastatin, erlotinib and indomethacin) the derivatization was expected to interfere with the binding to the drug's primary target, we used these derivatives to search for additional targets. It should be noted that for target deconvolution purposes it is important to test the BG derivatives in an appropriate assay to ensure that activity is retained or to prepare derivatives modified at different positions. We also included two negative controls in the Y3H screenings, BG and BG-(PEG)₄, that label SNAP-tag with a benzyl group and with a benzyl-polyethylene glycol (PEG) linker respectively. All BG drug derivatives and the two negative controls efficiently labeled SNAP-tag *in vitro* (Supplementary Fig. 6b).

Various cDNA libraries prepared from human tissue are commercially available. However, certain proteins can be underrepresented in tissue-specific libraries¹³. To minimize the occurrence of underrepresented proteins, we transformed human cDNA libraries from diverse tissues in yeast strain 1A2 in preparation for Y3H screenings. Furthermore, we reduced the rate of false positives from certain cDNA libraries by performing a negative selection with 5-FOA before positive selection (Supplementary Fig. 7a,b).

We screened each drug derivative and the two controls against eight human cDNA library preparations for a total of 80 Y3H screens; 3,069 colonies grew on the selection plates and 849 of these showed growth dependence on the presence of the drug derivative (Supplementary Fig. 7c,d). The two negative controls did not yield a single colony that showed compound growth dependence in any of

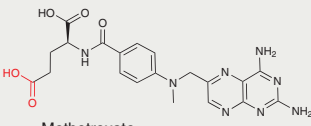
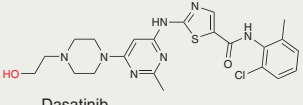
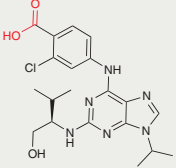
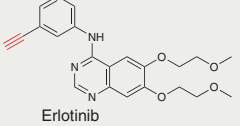
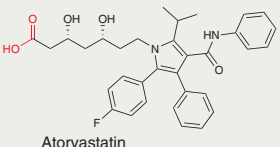
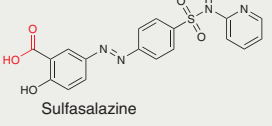
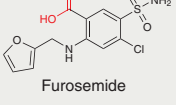
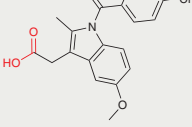
the eight libraries. This demonstrates that our SNAP-tag-based Y3H screenings generate few false positives (Supplementary Fig. 8a,b). We sequenced the cDNA library insert of all 849 Y3H hits and determined a total of 33 drug-protein interactions that were each represented between 1 and 237 times (Table 1 and Supplementary Fig. 8c,d). The following sections discuss the obtained results.

Methotrexate

Methotrexate is an antineoplastic antimetabolite with immunosuppressant properties that acts by potent inhibition of human DHFR (hDHFR) ($K_i = 5$ pM). We used this interaction as a positive control to test the efficacy of the SNAP-tag-based Y3H system. We identified a total of 173 hits dependent on the presence of the methotrexate derivative for growth; all 173 hits encoded hDHFR or a fragment thereof, demonstrating the efficacy of our Y3H system. Unexpectedly, we observed that no cDNA insert contained hDHFR in frame with GAL4AD (Supplementary Fig. 9a). Although it has been shown by others that out-of-frame fusion proteins can be detected in Y2H screenings¹⁵, we analyzed the efficiency of translational frameshifting in the SNAP-tag-based Y3H system by testing the ability of both hDHFR and eDHFR fused in all three possible reading frames to GAL4AD to activate transcription of the reporter gene in a methotrexate-DHFR Y3H growth assay. All constructs (except eDHFR in the +1 reading frame) showed a similar performance in the Y3H growth assay (Supplementary Fig. 9b).

Furthermore, we observed a reduced growth rate of both in-frame constructs compared with the out-of-frame constructs on nonselective plates. This reduced fitness could deplete the in-frame clone from the libraries. Taken generally, these results indicate that cDNA inserts in all three reading frames can encode true interactors and that the toxicity of cDNA inserts could be attenuated by reducing the expression level through frameshifts (Supplementary Fig. 9c).

Table 1 | Chemical structures of the compounds used in this study and the corresponding protein targets identified using the yeast-based platform for drug profiling.

Compound ^a	Protein target ^b
 Methotrexate	DHFR (173×)
 Dasatinib	LCK (138×) HADH (62×) FYN (38×) ^c FGR (34×) BTK (6×) CSK (5×) EPHA4 (3×) EPHB3 (3×) TEC (3×) EPHA2 (2×) EPHB2 (2×) FRK (2×) KIT (2×) EPHB4 (1×) ABL2 (1×) DDR1 (1×) MAPK14 (1×)
 Purvalanol B	PTK2B (4×) ^c FYN (3×) CABLES1 (2×) ^c CLK2 (2×) EPHA4 (1×)
 Erlotinib	ORP7 (17×) ^c
 Atorvastatin	PDE6D (237×) ^c NQO2 (29×) ^{c,d} ABR (16×) ALDH1A2 (2×) ALDH1A3 (2×) TBK1 (1×) COQ9 (1×)
 Sulfasalazine	SPR (3×) ^{c,d}
 Furosemide	CAII (6×)
 Indomethacin	

^aDrugs were linked to O⁶-benzylguanine at the functional group highlighted in red. ^bThe number of hits displayed for each protein target represents the total number of independent yeast colonies identified during the cDNA library screenings. Protein targets marked in bold are previously known targets. ^cDrug targets validated in this study by affinity chromatography. ^dDrug targets validated in this study in an activity assay.

Kinase inhibitors dasatinib, purvalanol B and erlotinib

Dasatinib is an ATP-competitive tyrosine kinase inhibitor used in the treatment of chronic myelogenous leukemia. We identified in our screenings 16 protein kinases and kinase domains as targets of dasatinib (Table 1). Dasatinib has been extensively profiled using a variety of methods, including direct binding assays with 287 recombinant kinases¹⁶. The drug binds to a total of 86 kinases ($K_D < 10 \mu\text{M}$), 40 with high affinity ($K_D < 30 \text{nM}$). All 16 kinases identified in our screening have a reported K_D for dasatinib below 30 nM. We reasoned that only high-affinity interactions were detected in our screening, as the drug needs to compete in the cell with millimolar concentrations of ATP. Having identified 40% of the subset of tight-binding kinases, we compared our results with two existing studies for target identification of dasatinib (Supplementary Table 1). One study used a quantitative chemical proteomics methodology that analyzes the competition between a drug and a mixed kinase-inhibitor affinity resin ('Kinobeads') by quantitative mass spectrometry¹⁷ to identify 17 of the 40 high-affinity binders. The other study used covalently immobilized dasatinib in chemical proteomics experiments to identify 20 of the 40 high-affinity binders as targets of dasatinib¹⁸. Both chemical proteomics approaches were more successful in identifying weak dasatinib-kinase interactions, presumably due to more favorable ratios of derivatized drug to ATP in lysates. Pair-wise comparison of the three data sets shows that the two chemical proteomics studies share the greatest similarity (Supplementary Table 1). This observation reflects the fact that Y3H screening of cDNA libraries allowed the identification of fragments encoding the soluble kinase domain of several transmembrane receptor tyrosine kinases. Entire integral membrane proteins are difficult to identify in both chemical proteomics experiments and Y3H screenings.

Five of the cDNA libraries used in the dasatinib Y3H screenings provided unique hits (Supplementary Table 2), thus emphasizing the importance of using cDNA libraries from different tissues. As a significant number of dasatinib hits were out of frame (Supplementary Table 2), we believe that the resulting attenuated expression level of potentially toxic human cDNA inserts such as kinases favors the isolation of out-of-frame inserts.

Finally, we identified an out-of-frame insert encoding hydroxycyl-coenzyme A dehydrogenase (HADH) from four different cDNA libraries, but no interaction between HADH and dasatinib was detected in validation experiments (Supplementary Fig. 10a,b). We speculate that a ternary complex between dasatinib, the in-frame peptide and a yeast kinase might be responsible for the selection of the out-of-frame HADH insert (Supplementary Fig. 10a–c).

Purvalanol B was developed for inhibition of cyclin-dependent kinases (CDKs); however, it also binds to other kinases¹⁷. We isolated a number of kinases that have also been identified by others (Table 1 and Fig. 3a)^{5,17}. Notably, we identified an indirect interaction between purvalanol B and CDK5 and ABL1 enzyme substrate 1 (CABLES1) in yeast cells. Indeed, immobilized purvalanol B efficiently isolated CABLES1 from a mammalian cell extract but failed to isolate it from a bacterial extract (Supplementary Fig. 10d). This observation suggests that the Y3H interaction is bridged through a yeast protein kinase, such as CDK2 or CDK5, and that Y3H screenings can also capture indirect binders.

Erlotinib is a drug used in the treatment of non-small cell lung cancer and pancreatic cancer; it is a reversible ATP-competitive inhibitor of epidermal growth factor receptor (EGFR). We derivatized erlotinib at its terminal alkyne moiety even though structural information suggested that this should interfere with its binding to EGFR and other kinases¹⁹. In concordance, we were not able to isolate kinases from Y3H selections using this erlotinib derivative, but we identified oxysterol-binding protein-related protein 7 (ORP7) as the first, to our knowledge, nonkinase target of the drug. We confirmed the binding of BG-derivatized and underivatized erlotinib to ORP7 using a pulldown assay

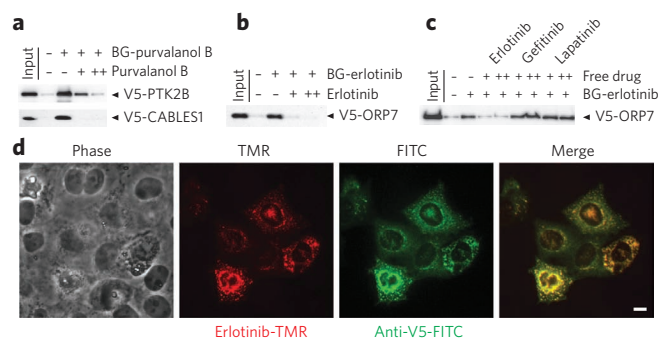


Figure 3 | Analysis of hits obtained from purvalanol B and erlotinib profiling. (a) A purvalanol B affinity matrix was prepared by binding of GST-SNAP to glutathione beads and reaction of SNAP-tag with BG-purvalanol B. A lysate of human U2OS cells expressing V5 epitope-tagged PTK2B or CABLES1 was incubated with the purvalanol B affinity matrix. Protein bound to the affinity matrix was analyzed by immunoblotting with a horseradish peroxidase (HRP)-labeled anti-V5 antibody. For competition experiments, the lysate was preincubated with underivatized purvalanol B (10 μM (+) or 100 μM (++)). (b) An erlotinib affinity matrix was prepared by binding of GST-SNAP to glutathione beads and reaction of SNAP-tag with BG-erlotinib. A pull-down assay of V5-ORP7 was performed in an analogous way to that described above. (c) Analysis of the binding of underivatized EGFR inhibitors to ORP7 in a competition pull-down assay. A lysate of human U2OS cells expressing V5-ORP7 was preincubated with erlotinib, lapatinib or gefitinib (10 μM (+) or 100 μM (++)) before performing a pull-down assay as described above. Full blots are available in **Supplementary Figure 14a**. (d) Micrographs showing colocalization of a fluorescent erlotinib derivative with epitope-tagged ORP7. Fixed and permeabilized human U2OS cells expressing V5-ORP7 were stained with a tetramethylrhodamine (TMR) derivative of erlotinib (erlotinib-TMR) and with an anti-V5-fluorescein antibody conjugate (anti-V5-FITC). The cells were imaged by wide-field fluorescence microscopy. Scale bar, 10 μm .

(Fig. 3b). In contrast, we observed that neither gefitinib nor lapatinib, two other specific EGFR inhibitors, were able to bind ORP7 (Fig. 3c). We next prepared a fluorescent derivative of erlotinib (erlotinib-TMR) and used it in fluorescence colocalization experiments. In fixed and permeabilized human U2OS cells, we observed colocalization of erlotinib-TMR with epitope-tagged ORP7 (Fig. 3d and **Supplementary Fig. 11a,b**). Finally, we analyzed the binding of erlotinib-TMR to recombinant ORP7 in fluorescence polarization experiments ($K_D = 230$ nM, **Supplementary Fig. 11c,d**). Furthermore, we observed that underivatized erlotinib efficiently competes for binding to ORP7 ($IC_{50} = 100$ nM, **Supplementary Fig. 11e**).

ORP7 is one of 12 members of the ORP family. ORPs are associated with diverse cellular functions such as control of lipid synthesis, transport and metabolism, transport of sterols and modulation of signal transduction; however, the function of individual ORP family members is not well characterized²⁰. ORP7 is an 842-residue protein containing a sterol-binding domain at its C-terminal end (440–830). Notably, the shortest ORP7 hit isolated in the Y3H screenings comprised amino acids 440–842, indicating that the sterol-binding domain of ORP7 is involved in the interaction with erlotinib. As ORP7 is the first nonkinase target of erlotinib, this interaction and its physiological role merit further investigation. In addition, as the natural substrate and the physiological role of ORP7 are unknown, derivatized erlotinib represents an interesting tool compound.

Atorvastatin

Atorvastatin is a member of the statin drug class that is used for the treatment of hypercholesterolemia; it is a competitive inhibitor of

3-hydroxy-3-methylglutaryl-CoA reductase (HMG-CoA reductase). The HMG-like moiety of atorvastatin occupies the enzyme's active site, whereas the rigid hydrophobic part of the drug occupies a shallow nonpolar groove²¹. Although derivatization of atorvastatin at its carboxyl group interferes with binding to HMG-CoA reductase, we speculated that this derivative could allow the identification of off-targets. In this study, we indeed identified several off-targets of atorvastatin. The most abundant hits identified in the Y3H screenings were the delta subunit of retinal rod phosphodiesterase (PDE6D) and quinone reductase 2 (NQO2) (Fig. 4a). The interaction of atorvastatin with PDE6D and NQO2 has been reported in a patent application, although no details are provided as to how these interactions were identified²².

We confirmed the binding of atorvastatin to PDE6D in a pull-down assay using both epitope-tagged and endogenous protein (Fig. 4b and **Supplementary Fig. 12a**). We then tested the binding of eight other statins to PDE6D, finding that only atorvastatin can bind PDE6D (Fig. 4c). In addition to its role in the regulation of the activity of retinal rod phosphodiesterase, it has been suggested that PDE6D plays a broader role in cellular signaling²³. PDE6D binds protein members of the Ras, Rap, Rho and Rab families by accommodation of their prenyl groups in a hydrophobic pocket, in a way that is similar to that of guanine nucleotide dissociation inhibitors²³. We assume that atorvastatin binds to that hydrophobic pocket. The interaction of PDE6D with prenylated proteins affects their intracellular localization. As statins inhibit both the biosynthesis of cholesterol and isoprenoids, they reduce the prenylation of proteins and interfere with their membrane localization²⁴. There is an intriguing possibility that atorvastatin is directly affecting protein localization through binding to the prenyl-binding site of PDE6D.

NQO2 is a flavoprotein that catalyzes the reduction of quinones and is thought to be involved in metabolic reduction and xenobiotic detoxification²⁵. It has been shown that imatinib, a drug used in the treatment of chronic myelogenous leukemia, binds and inhibits NQO2 (half-maximal inhibitory concentration (IC_{50}) = 80 nM)²⁵. Here, we found that atorvastatin binds to NQO2 and inhibits the activity of NQO2, albeit with much weaker potency ($IC_{50} \sim 50$ μM) than imatinib (Fig. 4d and **Supplementary Fig. 12b**). The relatively high IC_{50} of atorvastatin for NQO2 raises the question whether this interaction is of physiological relevance.

Finally, we isolated hits encoding the GTPase-activating domain of active breakpoint cluster region-related protein (Abr), two members of the retinaldehyde dehydrogenase family (ALDH1A2 and ALDH1A3), ubiquinone biosynthesis protein COQ9, and a C-terminal fragment of TANK-binding kinase 1 (TBK1). Although we confirmed these Y3H hits in retransformed yeast cells (Fig. 4a), the interaction of atorvastatin with these proteins could not be validated in pull-down assays (**Supplementary Fig. 12c,d**). Further experiments are needed to evaluate the significance of these findings.

Sulfasalazine

Sulfasalazine is an anti-inflammatory drug used against inflammatory bowel diseases (IBDs) such as ulcerative colitis, as well as against rheumatoid arthritis. Despite its medical importance, the mechanism of action of sulfasalazine remains obscure. Sulfasalazine is incompletely absorbed from the small intestine and carried to the colon where it is reduced by bacteria to sulfapyridine and mesalamine²⁶. The therapeutic effect of sulfasalazine in IBDs results, at least partially, from the topical release of mesalamine in the colon. It has been suggested that the anti-inflammatory activity of mesalamine is because of its binding to peroxisome proliferator-activated receptor- γ (PPAR- γ)²⁷. Sulfasalazine and mesalamine, however, differ in their therapeutic properties in IBDs, as sulfasalazine shows superior efficacy in maintaining remission of ulcerative colitis²⁸. More importantly, only sulfasalazine shows efficacy against rheumatoid arthritis. The differences between sulfasalazine and mesalamine could be due

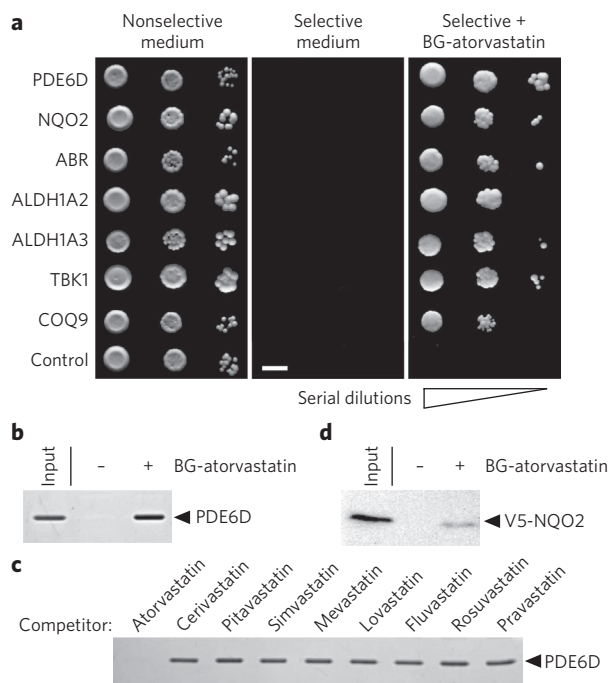


Figure 4 | Analysis of hits obtained from atorvastatin profiling.

(a) The binding of atorvastatin to a number of human proteins was identified in SNAP-tag-based Y3H screenings and subsequently confirmed in retransformed yeast cells. Yeast cells coexpressing LexA-SNAP and GAL4AD-X (X = PDE6D, NQO2, ABR, ALDH1A2, ALDH1A3, TBK1 or COQ9) were spotted on selective medium both in the presence and the absence of BG-atorvastatin. Scale bar, 5 mm. (b) An atorvastatin affinity matrix was prepared by binding of GST-SNAP to glutathione beads and reaction of SNAP-tag with BG-atorvastatin. Recombinant PDE6D was incubated with the affinity matrix and protein bound to the matrix was analyzed by SDS-PAGE and Coomassie staining. (c) The binding of various statins to PDE6D was tested in a competition binding assay. Recombinant PDE6D (2.5 μ M) was preincubated with underivatized statin (100 μ M) before incubation with the atorvastatin affinity matrix. Protein bound to the matrix was analyzed by SDS-PAGE and Coomassie staining. The absence of PDE6D bound to the affinity matrix indicates binding of the underivatized statin to PDE6D. (d) A lysate of human U2OS cells expressing V5 epitope-tagged NQO2 was incubated with the atorvastatin affinity matrix. Protein bound to the affinity matrix was analyzed by immunoblotting with a HRP-labeled anti-V5 antibody. Full gels and blots are available in **Supplementary Figure 14b**.

to their respective pharmacokinetics; alternatively, sulfasalazine or sulfapyridine could have additional targets^{29,30}.

In the SNAP-tag-based Y3H screenings, we identified the enzyme septipterin reductase (SPR) as a target of sulfasalazine (Fig. 5a). We confirmed the binding of BG-derivatized and underivatized sulfasalazine to SPR in a pull-down assay using epitope-tagged and endogenous SPR (Fig. 5b,c). SPR catalyzes the NADPH-dependent reduction of pyruvoyl-tetrahydropterin to tetrahydrobiopterin (BH4), this being the final step in the biosynthesis of the cofactor BH4 (ref. 31). BH4 is used by hydroxylases that are involved in the biosynthesis of tyrosine, dopamine and serotonin; it is also used by glyceryl ether monooxygenases that generate lipids that are involved in signal transduction. Finally, all nitric oxide synthases (NOS) require a tightly bound BH4 for activity. We next studied the inhibition of recombinant SPR by sulfasalazine in an activity assay (Supplementary Methods), finding that underivatized sulfasalazine inhibited SPR with an IC_{50} of 23 nM (Fig. 5d). By comparison, the known SPR inhibitor *N*-acetylserotonin ($K_i = 0.12 \mu$ M)³² had an IC_{50}

of 3.1 μ M in the same conditions. The principal metabolites of sulfasalazine also inhibited SPR although with lower potency: sulfapyridine and *N*-acetylsulfapyridine inhibited SPR with IC_{50} s of 480 nM and 290 nM, respectively, whereas mesalamine inhibited SPR with an IC_{50} of 370 μ M (Fig. 5d). In comparison, the reported IC_{50} value of mesalamine for PPAR- γ in a competitive binding assay is 15.2 mM²⁷. We next measured the effect of sulfasalazine and its metabolites on intracellular, total biopterin levels in a cellular assay (Supplementary Methods). At submillimolar concentrations, sulfasalazine, sulfapyridine and *N*-acetylsulfapyridine effectively reduced intracellular biopterin levels, indicating inhibition of BH4 biosynthesis (Fig. 5e). Sulfapyridine and *N*-acetylsulfapyridine show higher activity in the cellular assay relative to sulfasalazine, reflecting the fact that sulfasalazine is a known substrate of efflux pumps³³. Consistent with its lower *in vitro* inhibitory activity, mesalamine affects BH4 biosynthesis at higher concentrations (>1 mM). Overall, the data demonstrate that sulfasalazine and its metabolites are inhibitors of SPR *in vitro* and in cell culture. We propose that the inhibition of BH4 biosynthesis by sulfasalazine and its metabolites is crucially involved in the mechanism of action of the drug. Our reasoning is based on the demonstration that inhibitors of BH4 biosynthesis have been shown to reduce the production of nitric oxide (NO) in various inflammatory models^{34,35}. Both increased NO levels and increased inducible NOS (iNOS) activity have been associated with rheumatoid arthritis³⁶ and IBDs respectively³⁷, and selective iNOS inhibitors reduced inflammation both in rheumatoid arthritis³⁸ and ulcerative colitis³⁹ models.

The concentrations of sulfasalazine and its metabolites required for inhibition of BH4 biosynthesis in the cellular assay are within the range of their *in vivo* concentrations. The combined concentration of sulfapyridine and *N*-acetylsulfapyridine in serum and in synovial fluid during standard sulfasalazine therapy is around 100 μ M⁴⁰; the corresponding values for sulfasalazine and mesalamine are both around 15 μ M⁴⁰. Sulfapyridine is likely to be the active component of sulfasalazine in rheumatoid arthritis in view of its efficient BH4 biosynthesis inhibition in cell culture and the concentrations mentioned above. Indeed, it has been reported that sulfapyridine alone also shows efficacy against rheumatoid arthritis⁴¹.

With respect to IBDs, the intraluminal colonic concentration of mesalamine during sulfasalazine therapy is around 14 mM, as most of sulfasalazine is carried to the colon⁴². Even higher intraluminal colonic concentrations are reached with mesalamine formulations for topical delivery⁴³. Given the high intraluminal concentrations and the BH4 biosynthesis inhibitory profiles of sulfasalazine and its metabolites, it is possible that all contribute to inhibition of BH4 biosynthesis in the colonic epithelium, thereby complementing other mechanisms of action of mesalamine in IBDs.

Furosemide and indomethacin

Furosemide is a diuretic that is used to treat excessive fluid accumulation and body swelling by reducing the reabsorption of electrolytes, primarily by inhibition of the $Na^+K^+-2Cl^-$ symporter. It also inhibits members of the carbonic anhydrase family⁴⁴. We identified carbonic anhydrase 2 as a target of furosemide but could not detect the $Na^+K^+-2Cl^-$ symporter in this study because it is an integral membrane protein and therefore cannot be expressed functionally in the nucleus of yeast cells.

Indomethacin is a nonsteroidal anti-inflammatory drug whose effect is primarily attributed to nonselective inhibition of cyclooxygenase 1 (COX-1, $K_i = 0.016 \mu$ M) and 2 (COX-2, $K_i = 5 \mu$ M)⁴⁵. The derivatization of indomethacin with BG at its carboxyl group should disrupt the interaction with its main targets⁴⁶. In concordance, we were not able to detect these interactions in the Y3H screenings. The results obtained with furosemide and indomethacin illustrate two shortcomings and define future challenges of the Y3H approach: the inability to detect integral membrane protein targets and the need to derivatize the drug of interest.

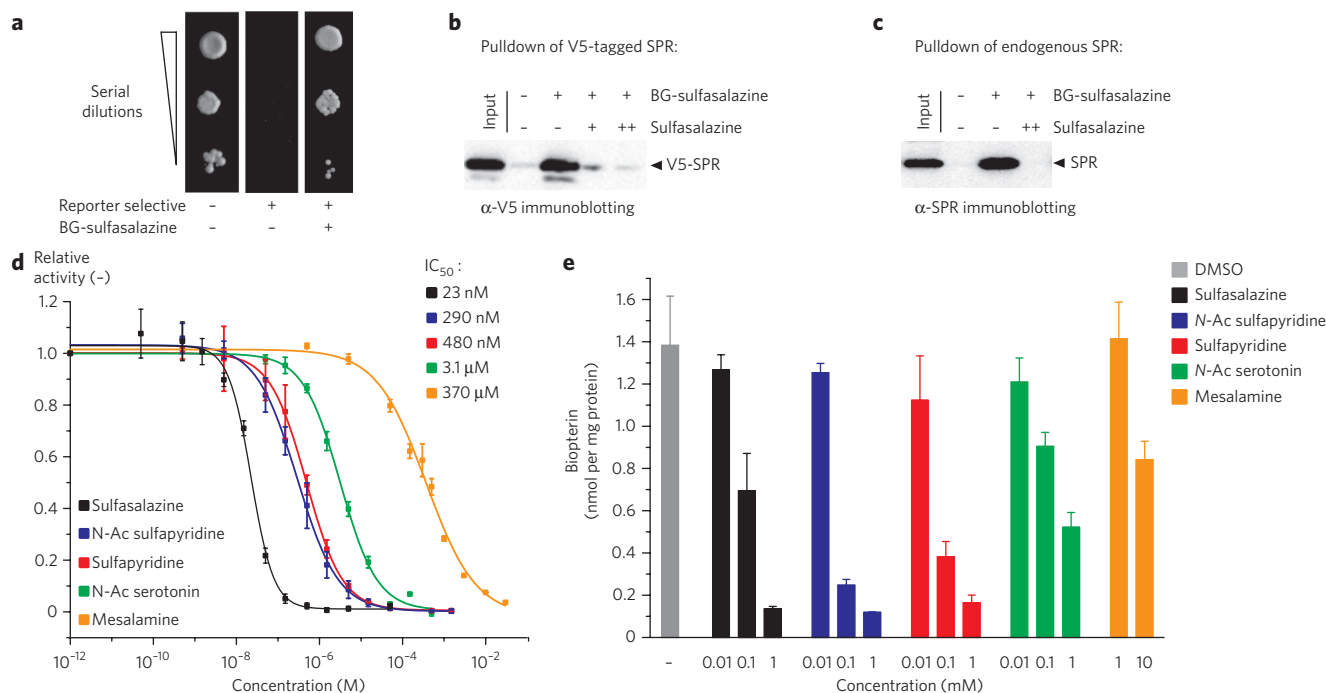


Figure 5 | Analysis of the interaction of sulfasalazine with SPR. (a) Yeast cells coexpressing LexA-SNAP and GAL4AD-SPR are dependent on the presence of BG-sulfasalazine for growth on selective medium. (b) A sulfasalazine affinity matrix was prepared by binding of GST-SNAP to glutathione beads and subsequent reaction with BG-sulfasalazine. A lysate of U2OS cells expressing V5-SPR was incubated with the matrix. Bound protein was analyzed by immunoblotting with HRP-labeled anti-V5 antibody. (c) A lysate of HEK 293 cells was incubated with the sulfasalazine matrix. Bound protein was analyzed by immunoblotting with anti-SPR primary antibody and HRP-labeled secondary antibody. For competition experiments, cell lysates were preincubated with sulfasalazine (10 μ M (+) or 100 μ M (++)). Full blots are available in **Supplementary Figure 14c**. (d) The inhibitory activities of sulfasalazine, sulfapyridine, *N*-acetylsulfapyridine (*N*-Ac sulfapyridine), mesalamine and *N*-acetylserotonin (*N*-Ac serotonin) against human SPR were measured in a spectrophotometric assay. The activity of SPR was normalized between 0 (no enzyme) and 1 (no inhibitor). The relative activity of SPR was fitted to the concentration of inhibitor using a dose-response equation with variable slope. Data represent mean values \pm s.d. of triplicates. (e) The effect of SPR inhibitors on cellular total biopterin levels was analyzed in rat pheochromatocytoma PC12 cells using an assay based on liquid chromatography and fluorescence detection. Cells were incubated with SPR inhibitors in medium supplemented with 10 μ M sepiapterin. Rat and human SPR showed similar IC₅₀s toward sulfasalazine and its metabolites (**Supplementary Fig. 13**). Data represent mean values \pm s.d. of at least triplicates.

DISCUSSION

Here we describe a drug profiling methodology based on a sensitive Y3H system. The performance of our Y3H system is primarily based on (i) the engineering of the yeast reporter strain and (ii) the choice of SNAP-tag for anchoring and displaying the derivatized drug inside yeast cells. Together, these measures allowed the generation of hits of high confidence; for example, all 173 hits isolated from the selections with methotrexate encoded hDHFR. From a practical standpoint, Y3H screenings offer a number of features that make them attractive for drug profiling. First, cDNA libraries from various tissues and species validated for the Y2H system can be employed and are commercially available. The screening results of dasatinib demonstrated the importance of testing multiple cDNA libraries, as this increased the number of target proteins uncovered. We also anticipate that, as in the case of Y2H experiments, array-based screens could further increase the performance of the system¹³. A second attractive feature of Y3H screenings is that the same pretransformed yeast stocks can be used repeatedly for screenings with different drugs, thus greatly simplifying the screening procedure. Finally, Y3H screenings do not require advanced instrumentation or special expertise. Disadvantages of the Y3H approach include the necessity to derivatize the drug of interest, its restriction to membrane-permeable drugs and its restriction to proteins or domains that can be functionally expressed in the nucleus of yeast. The wide range of applications of the SNAP-tag technology enables additional uses for the BG drug derivatives. In particular, coupling of the drug derivatives to GST-SNAP enabled the use of the same

drug derivatives for affinity purifications. This opens up the exciting possibility of running Y3H screenings and chemical proteomics experiments in parallel.

In this study, we identified new binding partners for approved drugs. We found the first nonkinase target of the EGFR inhibitor erlotinib, ORP7. We also characterized off-targets of the popular HMG-CoA reductase inhibitor atorvastatin, suggesting that atorvastatin has an affinity for certain isoprenoid-binding proteins such as PDE6D. The most intriguing finding of this work is that the popular anti-inflammatory drug sulfasalazine and its metabolites, sulfapyridine and mesalamine, are inhibitors of the enzyme SPR. Despite its long use and clinical importance in the treatment of IBDs and rheumatoid arthritis, its mechanism of action is not understood. The inhibition of SPR by sulfasalazine and its metabolites and a resulting decrease in BH₄ biosynthesis provides an attractive explanation for some of the drug's properties and suggests new and improved therapies. Genetic or chemical inhibition of the biosynthesis of the cofactor BH₄ is known to affect the activity of NOS^{34,35,47}. Increased activity of NOS has been associated with IBDs, and chemical inhibition of NOS has been shown to reduce inflammation in acute experimental colitis³⁹. Inhibition of SPR by sulfasalazine and its metabolites should therefore affect BH₄ levels, leading to reduced NOS activity in the gastrointestinal tract, providing a potential explanation for the efficacy of sulfasalazine in the treatment of IBDs. Increased NOS activity is also observed in rheumatoid arthritis³⁶, and inhibition of BH₄ biosynthesis by sulfasalazine and its metabolites should result in an attenuation of that activity.

A specific inhibition of BH4 biosynthesis also suggests new therapeutic applications for this drug. For example, cancer patients with a reduced-function haplotype in BH4 biosynthesis show a delayed need for opioid therapy⁴⁸. Consequently, sulfasalazine might be effective in delaying pain in cancer patients. The observation that sulfasalazine blocks the development of tactile allodynia in diabetic rats supports the hypothesis that sulfasalazine could be used for alleviation of chronic pain⁴⁹. Additionally, it has been shown that *N*-acetylserotonin, a less potent inhibitor of SPR than sulfasalazine and sulfapyridine *in vitro* and in cell culture, attenuated inflammatory pain in a rat model through inhibition of BH4 biosynthesis⁴⁷. Finally, our discovery that BH4 biosynthesis is inhibited by sulfasalazine might permit the suppression of some of its side effects by adjunct therapy, as it is possible that harmful side effects, such as anorexia, headache, nausea and vomiting may be caused by a change in the concentration of neurotransmitters dependent on BH4 for their biosynthesis. In consequence, these side effects might be attenuated by adjunct therapy with molecules (such as neurotransmitters, their biosynthetic precursors or reuptake inhibitors), which would restore a correct balance of neurotransmitters. The fact that patients with deficiency in SPR are responsive to treatment with *L*-dopa supports this hypothesis⁵⁰. Undoubtedly, the discovery that sulfasalazine and its metabolites are inhibitors of BH4 biosynthesis opens up a variety of exciting possibilities for this 70-year-old drug.

METHODS

Yeast strain and cDNA libraries. The reporter yeast strain 1A2 was derived from NMY51 (Dualsystems Biotech). 1A2 genotype: *MATa his3-Δ200 trp1-901 leu2-3,112 ade2 LYS2::(lexAop)₈-HIS3 ura3::(lexAop)₈-lacZ (lexAop)₈-ADE2 yor1::(lexAop)₈-URA3 GAL4 Δpdr5::loxP Δsnq2::loxP*. A description of the strain modification is available in the **Supplementary Methods**. Human cDNA libraries were from Clontech and from Dualsystems Biotech.

Preparation of library yeast stocks. SNAP-tag was cloned into vector pLexA-N (Dualsystems Biotech, **Supplementary Methods**). SNAP-tag was prepared in the lab of K. Johnsson. All details about the sequence and origin of SNAP-tag are given in the **Supplementary Methods**. The yeast strain 1A2 was transformed with the SNAP-tag bait plasmid according to standard procedures. The strain 1A2 + bait plasmid was then transformed with human cDNA libraries achieving at least 5×10^6 transformants per library (**Supplementary Methods**). The transformed cells were homogeneously spread (4-mm diameter glass beads) on 50 large plates (150-mm diameter) containing complete minimal medium minus leucine tryptophan (CM-LW). After 3 d at 30 °C, the yeast cells were resuspended in 1 × TE (10 mM Tris-Cl, 1 mM EDTA, pH 7.5) and pooled. The yeast cells were washed twice with one pellet volume 1 × TE and resuspended in one pellet volume freezing solution (65% (v/v) glycerol, 100 mM MgSO₄, 25 mM Tris-Cl pH 8). The yeast stocks were aliquoted and stored at -80 °C.

Negative preselection step. The viability of the pretransformed yeast stocks was determined by plating serial dilutions on CM-LW (in general, 4×10^8 – 7×10^8 colony forming units (c.f.u.) per ml). A volume of yeast stock containing 6×10^7 viable yeast cells was diluted in 1 × TE and spread homogeneously onto 20 large plates (150-mm diameter) containing CM-LW + 0.25 g l⁻¹ 5-FOA (20 mg l⁻¹ uracil, 1% (w/v) agarose). After 3 d at 30 °C, the yeast cells were resuspended in 1 × TE and pooled. The yeast cells were washed twice with one pellet volume 1 × TE, resuspended in one pellet volume freezing solution and stored at -80 °C.

Y3H selections. Each Y3H selection (one drug derivative versus one cDNA library) was performed on one large plate (150-mm diameter) containing complete minimal medium minus histidine leucine tryptophan (CM-HLW) + 2.5 mM 3-amino-1,2,4-triazole (3-AT) + 10–20 μM BG drug derivative (diluted from a 10–20 mM stock in DMSO) + 1% (w/v) agarose, pH 6.5. Then, 5–25 μl thawed yeast stock (1×10^8 – 7×10^8 c.f.u. per ml) was diluted in 1 × TE and homogeneously spread on the selection plates. After 10 d at 30 °C, all colonies larger than 1 mm in diameter were picked and resuspended in 250 μl 1 × TE in 96-well plates. Using a metal 96-prong replicator, the resuspended colonies were transferred onto CM-LW. After 4 d at 30 °C, the arrayed colonies were transferred back to 250 μl 1 × TE in 96-well plates. We spotted 2 μl of the resuspended yeast cells each on CM-LW, CM-HLW + 1 mM 3-AT + 0.1% (v/v) DMSO + 1.5% (w/v) agarose, pH 6.5, and CM-HLW + 1 mM 3-AT + 5–10 μM drug derivative + 1.5% (w/v) agarose, pH 6.5 using an eight-channel pipette. Colonies showing drug derivative growth dependence were grown in 0.85 ml CM-LW in 96-well deep well plates. After growth until saturation, the yeast cultures were centrifuged at 1,000g

for 10 min. The yeast pellets were resuspended in 200 μl zymolyase solution (1.2 M sorbitol, 100 mM sodium phosphate pH 7.4, zymolyase 20T 2 mg ml⁻¹) and incubated at 37 °C for 90 min with shaking. Plasmid DNA was then isolated with a commercial kit according to the manufacturer's instructions (NucleoSpin M-96 Plus Plasmid, Macherey-Nagel). The cDNA inserts were amplified by PCR and analyzed by sequencing (Macrogen). The cDNA identity was determined by BLAST analysis.

SNAP-tag-based GST pulldown. The open reading frames of the proteins of interest were inserted in vector pCDNA3.1/nV5-DEST (Invitrogen) for N-terminal V5-tagged protein expression by Gateway recombination from relevant entry clones. U2OS cells (maintained in DMEM supplemented with 10% (v/v) FBS) were transfected with the resulting constructs using Lipofectamine 2000 (Invitrogen) in 3.5-cm dishes. After transient expression for 48 h, the cells were lysed on ice for 10 min in buffer A (50 mM Tris-Cl pH 7.9, 150 mM NaCl, 5 mM EDTA, 1% (v/v) Triton X-100, 50 mM NaF, 1 mM Na₃VO₄, protease inhibitor cocktail (Complete Mini, Roche)). The lysate was cleared by centrifugation at 16,000g for 10 min at 4 °C and used as input sample in subsequent pulldown experiments. For the preparation of the pulldown matrix, 20 μl of 20% (v/v) glutathione Sepharose 4B slurry (GE Healthcare) in buffer B (50 mM Tris-Cl pH 7.9, 0.5 M NaCl) was mixed with an *Escherichia coli* lysate containing bead-saturating amounts of recombinant GST-SNAP for 30 min at 4 °C. After washing twice with 200 μl buffer A and resuspension in 50 μl buffer A, the immobilized GST-SNAP was labeled with the drug derivative by addition of 0.5 μl of 1 mM drug derivative in DMSO. After 30 min at room temperature, the beads were washed twice with 200 μl buffer A and then incubated with 50 μl mammalian protein extract for 1–3 h at 4 °C. For competition experiments, 0.5 μl of 1 or 10 mM underivatized drug in DMSO was added to the extract and incubated for 30 min on ice. After washing three times with 200 μl buffer A, bound protein was eluted in 20 μl 50 mM Tris-Cl pH 7.9 + 10 mM reduced glutathione. Eluted proteins were resolved by SDS-PAGE and transferred to a PVDF membrane. Immunoblotting was performed using anti-V5-HRP (Invitrogen), ECL Plus Western Blotting Detection Reagents (GE Healthcare) and a Kodak Image Station 440CF. In the blots, the input lane corresponds to 5–10% of the protein used in the pulldown assay. For experiments using endogenous protein levels, a lysate of HEK 293 cells (10–15 μg μl⁻¹) was prepared in the same way as for U2OS cells. Immunoblotting was performed using a rabbit anti-SPR antibody (Abcam ab96027) or a mouse anti-PDE6D antibody (Abcam ab55563) and an appropriate HRP-labeled secondary antibody.

Received 13 July 2010; accepted 22 February 2011;
published online 17 April 2011

References

1. Terstappen, G.C., Schlupen, C., Raggiacchi, R. & Gaviraghi, G. Target deconvolution strategies in drug discovery. *Nat. Rev. Drug Discov.* **6**, 891–903 (2007).
2. Chan, J.N., Nislow, C. & Emili, A. Recent advances and method development for drug target identification. *Trends Pharmacol. Sci.* **31**, 82–88 (2010).
3. Rix, U. & Superti-Furga, G. Target profiling of small molecules by chemical proteomics. *Nat. Chem. Biol.* **5**, 616–624 (2009).
4. Licitra, E.J. & Liu, J.O. A three-hybrid system for detecting small ligand-protein receptor interactions. *Proc. Natl. Acad. Sci. USA* **93**, 12817–12821 (1996).
5. Becker, F. *et al.* A three-hybrid approach to scanning the proteome for targets of small molecule kinase inhibitors. *Chem. Biol.* **11**, 211–223 (2004).
6. Keppler, A. *et al.* A general method for the covalent labeling of fusion proteins with small molecules *in vivo*. *Nat. Biotechnol.* **21**, 86–89 (2003).
7. Kolaczowski, M., Kolaczowska, A., Luczynski, J., Witek, S. & Goffeau, A. *In vivo* characterization of the drug resistance profile of the major ABC transporters and other components of the yeast pleiotropic drug resistance network. *Microb. Drug Resist.* **4**, 143–158 (1998).
8. McMurray, M.A. & Thorner, J. Septin stability and recycling during dynamic structural transitions in cell division and development. *Curr. Biol.* **18**, 1203–1208 (2008).
9. Bolin, J.T., Filman, D.J., Matthews, D.A., Hamlin, R.C. & Kraut, J. Crystal structures of *Escherichia coli* and *Lactobacillus casei* dihydrofolate reductase refined at 1.7 Å resolution. I. General features and binding of methotrexate. *J. Biol. Chem.* **257**, 13650–13662 (1982).
10. Gendrezig, S., Kindermann, M. & Johnsson, K. Induced protein dimerization *in vivo* through covalent labeling. *J. Am. Chem. Soc.* **125**, 14970–14971 (2003).
11. Mayer, R.J., Chen, J.T., Taira, K., Fierke, C.A. & Benkovic, S.J. Importance of a hydrophobic residue in binding and catalysis by dihydrofolate reductase. *Proc. Natl. Acad. Sci. USA* **83**, 7718–7720 (1986).
12. Murphy, D.J. & Benkovic, S.J. Hydrophobic interactions via mutants of *Escherichia coli* dihydrofolate reductase: separation of binding and catalysis. *Biochemistry* **28**, 3025–3031 (1989).
13. Koegl, M. & Uetz, P. Improving yeast two-hybrid screening systems. *Brief. Funct. Genomics Proteomics* **6**, 302–312 (2008).
14. Vidalain, P.O., Boxem, M., Ge, H., Li, S. & Vidal, M. Increasing specificity in high-throughput yeast two-hybrid experiments. *Methods* **32**, 363–370 (2004).

15. Fromont-Racine, M., Rain, J.C. & Legrain, P. Toward a functional analysis of the yeast genome through exhaustive two-hybrid screens. *Nat. Genet.* **16**, 277–282 (1997).
16. Karaman, M.W. *et al.* A quantitative analysis of kinase inhibitor selectivity. *Nat. Biotechnol.* **26**, 127–132 (2008).
17. Bantscheff, M. *et al.* Quantitative chemical proteomics reveals mechanisms of action of clinical ABL kinase inhibitors. *Nat. Biotechnol.* **25**, 1035–1044 (2007).
18. Rix, U. *et al.* Chemical proteomic profiles of the BCR-ABL inhibitors imatinib, nilotinib, and dasatinib reveal novel kinase and nonkinase targets. *Blood* **110**, 4055–4063 (2007).
19. Stamos, J., Sliwkowski, M.X. & Eigenbrot, C. Structure of the epidermal growth factor receptor kinase domain alone and in complex with a 4-anilinoquinazoline inhibitor. *J. Biol. Chem.* **277**, 46265–46272 (2002).
20. Fairn, G.D. & McMaster, C.R. Emerging roles of the oxysterol-binding protein family in metabolism, transport, and signaling. *Cell. Mol. Life Sci.* **65**, 228–236 (2008).
21. Istvan, E.S. & Deisenhofer, J. Structural mechanism for statin inhibition of HMG-CoA reductase. *Science* **292**, 1160–1164 (2001).
22. Lockhart, D.J. *et al.* Pyrrole compounds and uses thereof. Vol. US 7.323.490 B2 (Ambit BioSciences Corporation, 2008).
23. Wilson, S.J. & Smyth, E.M. Internalization and recycling of the human prostacyclin receptor is modulated through its isoprenylation-dependent interaction with the delta subunit of cGMP phosphodiesterase 6. *J. Biol. Chem.* **281**, 11780–11786 (2006).
24. Cordle, A., Koenigsknecht-Talboo, J., Wilkinson, B., Limpert, A. & Landreth, G. Mechanisms of statin-mediated inhibition of small G-protein function. *J. Biol. Chem.* **280**, 34202–34209 (2005).
25. Winger, J.A., Hantschel, O., Superti-Furga, G. & Kuriyan, J. The structure of the leukemia drug imatinib bound to human quinone reductase 2 (NQO2). *BMC Struct. Biol.* **9**, 7 (2009).
26. Caprilli, R., Cesarini, M., Angelucci, E. & Frieri, G. The long journey of salicylates in ulcerative colitis: the past and the future. *J. Crohn's Colitis* **3**, 149–156 (2009).
27. Rousseaux, C. *et al.* Intestinal antiinflammatory effect of 5-aminosalicylic acid is dependent on peroxisome proliferator-activated receptor-gamma. *J. Exp. Med.* **201**, 1205–1215 (2005).
28. Sutherland, L. & Macdonald, J.K. Oral 5-aminosalicylic acid for maintenance of remission in ulcerative colitis. *Cochrane Database Syst. Rev.* CD000544 (2006).
29. Baggott, J.E., Morgan, S.L., Ha, T., Vaughn, W.H. & Hine, R.J. Inhibition of folate-dependent enzymes by non-steroidal anti-inflammatory drugs. *Biochem. J.* **282**, 197–202 (1992).
30. Wahl, C., Liptay, S., Adler, G. & Schmid, R.M. Sulfasalazine: a potent and specific inhibitor of nuclear factor kappa B. *J. Clin. Invest.* **101**, 1163–1174 (1998).
31. Thöny, B., Auerbach, G. & Blau, N. Tetrahydrobiopterin biosynthesis, regeneration and functions. *Biochem. J.* **347**, 1–16 (2000).
32. Smith, G.K., Duch, D.S., Edelstein, M.P. & Bigham, E.C. New inhibitors of sepiapterin reductase. Lack of an effect of intracellular tetrahydrobiopterin depletion upon in vitro proliferation of two human cell lines. *J. Biol. Chem.* **267**, 5599–5607 (1992).
33. Dahan, A. & Amidon, G.L. MRP2 mediated drug-drug interaction: indomethacin increases sulfasalazine absorption in the small intestine, potentially decreasing its colonic targeting. *Int. J. Pharm.* **386**, 216–220 (2010).
34. Gross, S.S. & Levi, R. Tetrahydrobiopterin synthesis. An absolute requirement for cytokine-induced nitric oxide generation by vascular smooth muscle. *J. Biol. Chem.* **267**, 25722–25729 (1992).
35. Bune, A.J. *et al.* Inhibition of tetrahydrobiopterin synthesis reduces in vivo nitric oxide production in experimental endotoxemic shock. *Biochem. Biophys. Res. Commun.* **220**, 13–19 (1996).
36. Farrell, A.J., Blake, D.R., Palmer, R.M. & Moncada, S. Increased concentrations of nitrite in synovial fluid and serum samples suggest increased nitric oxide synthesis in rheumatic diseases. *Ann. Rheum. Dis.* **51**, 1219–1222 (1992).
37. Singer, I.I. *et al.* Expression of inducible nitric oxide synthase and nitrotyrosine in colonic epithelium in inflammatory bowel disease. *Gastroenterology* **111**, 871–885 (1996).
38. Connor, J.R. *et al.* Suppression of adjuvant-induced arthritis by selective inhibition of inducible nitric oxide synthase. *Eur. J. Pharmacol.* **273**, 15–24 (1995).
39. Kankuri, E. *et al.* Suppression of acute experimental colitis by a highly selective inducible nitric-oxide synthase inhibitor, N-[3-(aminomethyl)benzyl]acetamide. *J. Pharmacol. Exp. Ther.* **298**, 1128–1132 (2001).
40. Farr, M., Brodrick, A. & Bacon, P.A. Plasma and synovial fluid concentrations of sulphasalazine and two of its metabolites in rheumatoid arthritis. *Rheumatol. Int.* **5**, 247–251 (1985).
41. Pullar, T., Hunter, J.A. & Capell, H.A. Which component of sulphasalazine is active in rheumatoid arthritis? *Br. Med. J. (Clin. Res. Ed.)* **290**, 1535–1538 (1985).
42. Lauritsen, K., Hansen, J., Ryde, M. & Rask-Madsen, J. Colonic azodisalicylate metabolism determined by in vivo dialysis in healthy volunteers and patients with ulcerative colitis. *Gastroenterology* **86**, 1496–1500 (1984).
43. Klotz, U. Colonic targeting of aminosaliculates for the treatment of ulcerative colitis. *Dig. Liver Dis.* **37**, 381–388 (2005).
44. Temperini, C., Cecchi, A., Scozzafava, A. & Supuran, C.T. Carbonic anhydrase inhibitors. Comparison of chlorthalidone, indapamide, trichloromethiazide, and furosemide X-ray crystal structures in adducts with isozyme II, when several water molecules make the difference. *Bioorg. Med. Chem.* **17**, 1214–1221 (2009).
45. Gierse, J.K., Koboldt, C.M., Walker, M.C., Seibert, K. & Isakson, P.C. Kinetic basis for selective inhibition of cyclo-oxygenases. *Biochem. J.* **339**, 607–614 (1999).
46. Hori, T. *et al.* Crystal structure of anti-configuration of indomethacin and leukotriene B4 12-hydroxydehydrogenase/15-oxo-prostaglandin 13-reductase complex reveals the structural basis of broad spectrum indomethacin efficacy. *J. Biochem.* **140**, 457–466 (2006).
47. Tegeder, I. *et al.* GTP cyclohydrolase and tetrahydrobiopterin regulate pain sensitivity and persistence. *Nat. Med.* **12**, 1269–1277 (2006).
48. Lötsch, J., Klepstad, P., Doehring, A. & Dale, O.A. GTP cyclohydrolase 1 genetic variant delays cancer pain. *Pain* **148**, 103–106 (2010).
49. Berti-Mattera, L.N., Kern, T.S., Siegel, R.E., Nemet, I. & Mitchell, R. Sulfasalazine blocks the development of tactile allodynia in diabetic rats. *Diabetes* **57**, 2801–2808 (2008).
50. Blau, N., Bonafe, L. & Thony, B. Tetrahydrobiopterin deficiencies without hyperphenylalaninemia: diagnosis and genetics of dopa-responsive dystonia and sepiapterin reductase deficiency. *Mol. Genet. Metab.* **74**, 172–185 (2001).

Acknowledgments

We thank D. Auerbach (Dualsystems Biotech) for sharing plasmid pU6H3VSV, strain NMY51, BG-purvalanol B and cDNA libraries; N. Johnsson (Ulm University) for sharing plasmid pSH47; and O. Hantschel and G. Superti-Furga (Center for Molecular Medicine of the Austrian Academy of Sciences) for sharing plasmid pETM30-NQO2. We thank S. Moser, L. Reymond and C. Fellay for technical assistance. We acknowledge R. Chidley, M.J. Hinner and G. Lukinavicius for critically reading the manuscript. This work was supported by the Swiss National Science Foundation and the Federal Office for Professional Education and Technology.

Author contributions

C.C., H.H. and K.J. designed experiments and analyzed data, C.C. developed and performed yeast-based screens, H.H. and C.C. performed hit validation experiments, M.G.P. measured intracellular biopterin levels, E.M. synthesized drug derivatives, and C.C. and K.J. wrote the paper.

Competing financial interests

The authors declare no competing financial interests.

Additional information

Supplementary information is available online at <http://www.nature.com/naturechemicalbiology/>. Reprints and permissions information is available online at <http://www.nature.com/reprints/index.html>. Correspondence and requests for materials should be addressed to K.J.